Structural Characterization of Selected Pdases

Thesis for Departmental Honors in Chemistry and Biochemistry

Samantha Wellington

Committee Members:

Thesis Advisor
Dr. Bruce E. Eaton
Chemistry & Biochemistry

Honors Advisors
Dr. Hang (Hubert) Yin
Chemistry & Biochemistry

Dr. Norman R. Pace
Molecular, Cellular, & Developmental Biology

DATE
April 6, 2012

ACKNOWLEDGEMENTS

I would like to thank my advisor Dr. Bruce Eaton for his continual support and advice throughout this project. I would also like Jessica Rouge for her guidance both in terms of teaching physical techniques and providing research direction and insight, without which this project would never have been successful. Dr. Daniel Feldheim and the members of the Eaton Group also deserve acknowledgement for their input and support on this project and Dr. Norman Pace was hugely helpful in optimizing sequencing gel conditions. Finally, I would like to thank the Caruthers lab for the use of their UV-Vis spectrophotometer on which all melting experiments were completed.

ABSTRACT

A group of RNAs, referred to as Pdases, which mediate the formation of palladium nanoparticles was discovered through a SELEX process. The Pdases contain 5-(4-pyridylmethyl)-uracil residues without which they are incapable of mediating nanoparticle formation. From previous studies, it is clear that the structures of these RNA molecules play a role in substrate and product specificity, but it is unknown what those structures are and how they vary between the RNA aptamers and between modified and unmodified versions of the RNA. This thesis employs the techniques of thermal melting, circular dichroism, and RNase structure mapping to compare the structures of five selected Pdases to each other. From the melting experiments, it is evident that the Pdases have variable structures that are not formed exclusively from Watson Crick interactions. The Pdases also have different melting profiles if unmodified uracil residues are used in place of the modified bases. The sequences, in both modified and unmodified form, produce circular dichroism spectra characteristic of A-form helices. The spectra, however, are very different from each other in terms of amplitude suggesting that the base modifications affect the structure of the RNA. Finally, structure mapping controls have been completed and moving forward, the technique has the capability of providing more structural detail for the Pdases.

Introduction

Until the 1980s, the only known biological catalysts were proteins.[1] The first catalytic RNA, or ribozyme, was discovered by the Cech lab in 1982.[1-3] The research group found a self-splicing intron in *Tetrahymena* pre-rRNA. In the few years following this finding, a number of other ribozymes were discovered, including RNase P which expanded the idea of ribozymes to include multiple-turnover enzymes.[1, 2] Now, tens of naturally occurring ribozyme species have been identified.[3] X-ray crystallography has revealed that the catalytic function of RNA is dependent upon the molecule folding into a specific three-dimensional shape and, occasionally, metal ions and protein factors are involved in the folding of ribozymes.[2, 3] The known natural ribozymes are limited to phosphodiester chemistry, with the exception of the ribosome which carries out peptidyl transferase reactions.[2, 4]

While natural ribozymes are somewhat restricted in the diversity of their chemical reactions, numerous RNA catalysts have been obtained through *in vitro* selection.[2] These ribozymes are capable of catalyzing a great range of chemical reactions, including ester and amide bond formation, carbon-carbon bond formation, and porphyrin metallation.[2, 5, 6] Many of these ribozymes have been developed through SELEX, or the Systematic Evolution of Ligands by EXponential amplification.[3, 7] SELEX was initially developed for the discovery of nucleic acids with high-affinity for certain molecules including amino acids, antibiotics, and proteins.[7] The technique has since been expanded and applied to the discovery of ribozymes. In the basic SELEX technique, a pool of up to 10^{15} random DNA sequences is generated synthetically, then transcribed into RNA.[8] The library of random RNA sequences is exposed to a selection step that isolates molecules with the desired binding or chemical activity.[2] The "winners" are reversed transcribed into DNA and amplified by PCR. This DNA is transcribed into RNA and the selection steps are repeated, typically between 6

and 15 times.[8] The ability to select for RNA with a desired function and amplify it repetitively results in a final pool of RNA in which the RNA catalysts dominate.[6]

In discovering ribozymes, a limitation of natural RNA and DNA is the lack of diversity in functional groups as compared to proteins, but this constraint can be overcome by the use of modified bases.[9] In fact, not even natural nucleic acids are limited to the four most common bases – more than 70 RNA modifications have been identified in natural biology.[6] The incorporation of modifications on RNA bases greatly expands both the structural motifs and the functional capabilities available to RNA. RNA selections have been completed with various modified bases including bases with pyridyl and imidazole modifications.[6] In the SELEX technique, the modified base replaces its natural counterpart in the transcription procedure. This ensures the sequences always contain the same modifications and eliminates any complications involved in chemically modifying the RNA post-transcriptionally. T7 RNA Polymerase is capable of functioning with a variety of 5 position modifications on uridines, ensuring successful incorporation of these modified bases.[6, 9] In many cases, attempts to discover ribozymes using unmodified RNA were unsuccessful while on the other hand attempts using modified RNA generated catalytically active ribozymes. In one case, modified RNA was able to increase the rate of cycloaddition by up to 800-fold while RNA without the modification was completely inactive.[6] The incorporation of modified bases clearly expands the functionality of RNA and provides the ability to select for better RNA catalysts.

The Pdase Selection

In 2004, Lina Gugliotti, Daniel Feldheim, and Bruce Eaton published the results of a selection for RNA capable of mediating metal-metal bond formation.[10] The selection began with single-stranded synthetic DNA 87 bases in length, with a 40 base random region.[10] Two-cycle PCR was used to generate a dsDNA library which was transcribed into RNA using T7 RNA Polymerase.

The RNA was transcribed using ATP, CTP, GTP and 5-(4-pyridylmethyl)-uridine 5'-triphosphate (See Figure 1 for structure).[10] The modification on uridine was incorporated to provide additional metal coordination sites.[10, 11] The RNA library was then incubated with $[Pd_2(DBA)_3]$.[10, 11] RNA was selected if it did not flow through 100-kD molecular weight cutoff microcons. Molecules that mediated the formation of Pd particles and remained bound to the particles or molecules that simply bound particles were selected for by this technique.[10] The RNA was reverse transcribed and PCR amplified to complete the cycle (See Figure 1 for the complete cycle).[10]

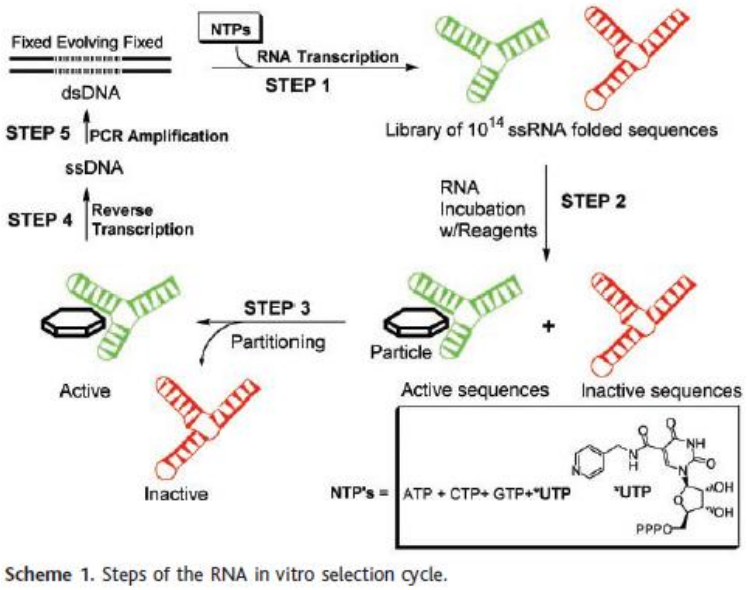

Figure 1. Selection scheme used for the Pdase SELEX.[10]

During cycles 4-8, the 100-kD molecular weight cutoff selection was followed by native polyacrylamide gel (6%) electrophoresis mobility shift-dependent partitioning. Slowly migrating bands that showed dependence on both Pd and RNA were isolated.[10] The selection was repeated for a total of eight cycles.

The selection resulted in groups of highly conserved sequences. The final Pdases were split into in four families based on conserved sequence regions; there were also three orphan sequences.[11]

Representative members from each family (Pd 17, Pd 19, Pd 20, and Pd 81) all mediate the formation of hexagonal nanoparticles.[10, 11] The family groupings are shown in Figure 2.

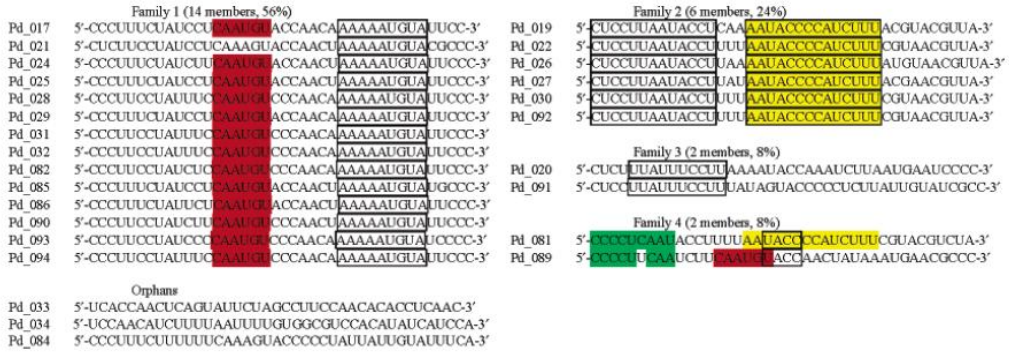

Figure 2. This table shows the sequence of the random regions and the family groupings of the Pdases.[11]

The hexagonal particles formed in the presence of the Pdase are unique in their large size and shape uniformity; the average particle size mediated by Pd 17 is 1.2 ± 0.6 μm.[10] One orphan sequence, Pd 34, was distinctive in that particle preparations using the Pdase yielded Pd cubes sized 0.1 μm ± 0.05 μm by 0.07μm ± 0.02 μm.[11] Representative particles mediated by Pd 17 and by Pd 34 are shown in Figure 3. Based on the results of the selection, it is believed that the evolution process resulted in RNAs that "reproducibly fold into intricate 3D structures dictated by their sequence", though those structures are yet to be elucidated.[11]

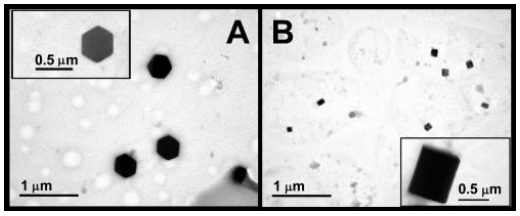

Figure 3 Representative Pd particles mediated by the Pdases. A. Hexagonal particles mediated by Pd 17. B. Cubic particles mediated by Pd 34.[11]

RNA Structure

RNA is capable of not only Watson-Crick base pairing, but also is capable of non-canonical base pairing. The large variety of motifs in RNA allows the molecule to fold into numerous different

structures, and mapping of these secondary and tertiary structures can provide an understanding of RNA functions.[12, 21] Based on experiments with truncated, unmodified, and thermally melted versions of the Pdases, it is clear that the full-length RNA molecules have three-dimensional structure that is important to forming the active site.[11] Replacing the pyridyl-modified RNA with native RNA for the Pd 17 and Pd 34 sequences resulted in a low yield of spherical particles, with no observable hexagonal or cubic particles.[11] This loss of RNA function was hypothesized to be caused by changes in RNA structure or by the absence of functional groups in the active site. Thermal denaturation of Pd 17 also resulted in a "loss of shape control and a low yield of solid material", further demonstrating the importance of RNA structure to the function of the Pdases.[11] Finally, when the 3' fixed region of Pd 17 was truncated, both spherical and hexagonal particles were formed, and truncating just 4 nucleotides into the variable region resulted in particles of undefined shape.[11] These results suggest that the fixed region of the RNA is important to the overall structure of the molecule and that the variable region is highly important to three dimensional structure and to metal-metal bond formation.

While structure is clearly essential to the function the Pdases, elucidating structures remains challenging. An RNA molecule only 80-nucleotides long can fold into up to 10^{48} different strctures.[12] Due to the unique folding properties of RNA, such as non-canonical base pairing, prediction of RNA structure is very difficult – current 2D prediction models are only about 70% accurate with 3D predictions and models of molecules containing base modifications obviously presenting even more challenges.[12] However, determining the structure of the Pdases will provide great insight into a number of issues. Structural characterization of the Pdases will allow for a deeper understanding of their functionality and generate ideas for future applications and studies of the RNAs. By comparing unmodified versions of the RNA to the modified Pdases, it will become clear if and how the pryidyl modifications affect RNA folding. The Pdases can also be compared to each other to determine if

the RNA molecules capable of mediating Pd particle formation are similarly structured or if a variety of structures are capable of this functionality. Ultimately, structural characterization will provide a better understanding of the Pdases and has the potential to lead to better design of aptamers or the ability to modify existing aptamers to create a desired functionality. Understanding the Pdases may also lead to the development of useful nanoscale materials. The shape, size, and composition of materials affects their effectiveness as potential catalysts.[26, 27] Because of this and the fact that understanding the Pdases could lead to even more control over palladium nanoparticle formation, these studies have the potential to lead to the development of palladium particles with desired catalytic properties.

In 2009, Hassan Azimi began research to determine the structures of the Pdases. His work studied the thermal melting and circular dichroism spectra of Pd 17 and Pd 34.[25] Azimi found that Pd 17 and Pd 34 likely have A-form structure and that Pd 17 is able to fold into secondary structures in 10% THF (palladium nanoparticles are prepared with the Pdases in THF).[25] The project presented in this thesis builds on that early work and employs thermal melting, circular dichroism, and RNase structure mapping to study structural features of the Pdases. Thermal melting experiments indicate the existence of secondary or higher order structure as well as the stability of the folded structure. Circular dichroism spectra can be compared to known spectra in order to determine secondary structure and structure mapping has the capability of providing a detailed picture of the structural elements in RNA. One Pdase from each family was chosen as a representative for the experiments; Pd 17, Pd 20, Pd 92, and Pd 81 were each chosen. Pd 34 was also included in the experiments due to its unique ability to mediate cubic particle formation. Pd 17, Pd 20, Pd92 and Pd 81 are all known to mediate hexagonal particle formation.[10]

Thermal Melting Background

When an oligonucleotide is heated, its absorbance of 260nm light increases.[13] This phenomenon, known as hyperchromicity, is due to changes in the overall dipole of the nucleic acid as it unfolds.[13] When the bases of a nucleic acid are stacked or paired, the dipole moment of each base induces a transition dipole in its neighboring bases. In stacked bases, the induced dipole is always opposite the transition dipole intrinsic to the base – the positive end of the transition dipole induces a negative charge and the negative end of the transition dipole induces a positive charge.[13] The sum of the transition dipoles and the induced dipoles is therefore less than the sum of the transition dipole of each individual base. When a nucleic acid unfolds, and the bases become unstacked, this reduction in overall dipole is eliminated. The extinction coefficient, ε, of a nucleic acid is proportional to the square of the transition dipole, thus relating the changes in dipole moment to the changes in absorbance ($a = \varepsilon lc$).[13] The direction of the transition dipoles in paired bases also leads to hyperchromicity. Thus, folded nucleic acids, overall, absorb less light than their native counterparts.

When a nucleic acid is melted, absorbance versus temperature can be plotted and analyzed for melting temperature, overall change in absorbance, and kinetic parameters. Duplex denaturation results in an increase in absorbance of about 15 to 20%.[14] Changes larger than this indicate a folded structure that more greatly reduces the dipole moment, potentially due to a more highly ordered structure. Thermal melting profiles are also often analyzed for T_m, which is the temperature of melting or the temperature of midtransition.[14] For double stranded molecules the T_m is the temperature at which half of the hydrogen bonds between the base pairs are broken.[14] T_m can be determined by two different methods. The first is by determining the midpoint of the melting curve. This technique is performed by drawing baselines that follow the absorbance before melting begins and after it's finished. A median line is then drawn between these two baselines and the T_m is taken

to be the point where the median line crosses the experimental melting curve.[14] This method has a level of uncertainty due to the subjective nature of baseline determination. An alternative to the midpoint method is to simply determine the inflection point of the experimental melting curve. This inflection point, found by calculating the maximum of the first derivative of the melting curve, is taken to be the melting transition, or T_m.[14] In this method, the determined T_m is only truly the melting temperature for an intramolecular equilibrium; i.e. the method is not accurate if the RNA folds via intermolecular interactions.[14]

It is possible for an experimental melting curve to have more than one transition. Additional transitions are typically due to the unfolding of tertiary structures more complex than a double helix. For example, multiple transitions are often observed in RNA that is folded into hairpins organized into a tertiary structure.[15] At a lower temperature, the tertiary structure unfolds and at higher temperatures a transition can be observed for the unfolding of each individual hairpin.[14]

Technique Considerations

When conducting thermal melting experiments, it is important to select an appropriate buffer: one with a pKa near the desired pH and a pKa that is not temperature dependent. For neutral pH, buffers such as cacodylate and acetate are best; phosphate buffer is also an acceptable buffer, though its pKa is slightly temperature dependent.[14]

The rate of temperature change is also a crucial parameter for the melting experiments. The structures of catalytic RNAs often include noncanonical base pairing and not all structures are as fast to form as Watson-Crick duplexes.[14] If the rate of temperature change is more rapid than the rate of RNA folding, it will lead to experimental results that do not represent equilibrium curves; it is for this reason melting experiments are often run at a temperature change rate of 0.5°C/min or 1°C/min.[14, 15, 28] If there is an observable difference between the melting curve obtained while temperature is increased and the curve obtained while temperature is decreased, the observed

melting curves are likely not the equilibrium curves. In this case, temperature gradients can be lowered in order to measure the melting transitions at equilibrium.[14]

Circular Dichroism (CD) Background

The circular dichroism (CD) spectra of nucleic acids can give more information about secondary structure than thermal melting curves because CD spectra have both sign and magnitude.[13] In the technique, the RNA is exposed to circularly polarized light, which produces a right- or left-handed helix in space. For absorption to occur the molecule exposed to the light must be achiral or there must be perturbations created by an asymmetric environment.[13] In the case of nucleic acids, the bases act as chromophores for the CD transition.[16] Absorption of the light is due to both the intrinsic CD of the nucleotide monomers and to the interaction of the base with neighboring bases, arranged asymmetrically about it.[16] The interaction between bases accounts for the majority of the CD spectrum, which is mainly dependent on base stacking geometry.[13] When the nucleic acid absorbs right- or left-hand circularly polarized light or both, the polarization of the light is changed to an elliptical polarization. The circular dichroism spectrophotometer reports CD activity in milidegrees which corresponds to an angle of the ellipse.[13] This CD data is normalized by converting to $\Delta\varepsilon$ which is equal to $\varepsilon_L - \varepsilon_R$ where ε is the molar extinction coefficient and has units M^{-1} cm^{-1}.[17] Molar extinction coefficient accounts for concentration of the nucleic acid and pathlength of the cuvette, allowing CD spectra to be compared for multiple samples.

Circular dichroism is most useful for comparing conformations and detecting changes in structure when temperature or solvent are changed.[13] By comparing the CD spectra of a sample of interest to spectra of RNA with known conformations, researchers can gain insight into the sample's secondary structure. The CD spectrum of A-form RNA typically has a large positive peak at 260nm and a deep negative band around 210nm.[13, 17, 18] A-DNA has a similar spectrum with a maximum at 270nm and a minimum near 210nm.[13] The peak at 260nm is somewhat variable in its exact position;

in some studies, the peak for A-form RNA was at 267nm rather than 260nm.[18] Additionally, the magnitude of the peak at 260nm is sensitive to winding angle of the nucleic acid.[13]

Calculating Error

In both circular dichroism and thermal melting, it is necessary to repeat experiments with multiple samples of the same nucleic acid in order to obtain accurate results. For T_m and for CD maxima and minima, values are calculated for each experiment and then averaged. Error is calculated by determining t-scores. While Z-scores, which are based on a normal distribution, are more common, they can only be accurately used when the population variance is known or when the sample size is greater than 30.[19] For the experiments in this study, measurements were taken at least three times to ensure reproducibility. While three repetitions is the standard in chemistry, the sample size is relatively small from a statistics perspective. The t-score method allows error to be calculated from the sample standard deviation instead of population standard deviation. Error for the experiments in this study was calculated using 90% confidence intervals where $error = \frac{S*t_{\alpha,v}}{\sqrt{n}}$ where S is the sample standard deviation, $t_{\alpha,v}$ is the t-score with $\alpha = 0.05$ for a 90% confidence interval and v is the degrees of freedom (equal to n-1), and n is the sample size. $t_{\alpha,v}$ is determined by using a table of standard values.[19]

Structure Mapping Background

Structure mapping has the capability to elucidate structural detail for nucleic acids up to 150 nucleotides in length.[20] Because the procedure relies on gel electrophoresis to separate RNA molecules, olgionucleotides longer than 150 bases cannot be resolved well using this technique. In the procedure, the sample is first end labeled. Typically, the 5' terminal phosphates of the RNA are removed with alkaline phosphatase, then replaced with ^{32}P using T4 polynucleotide kinase and γ-^{32}P-ATP.[20, 21] 3' end labeling is also a common technique. The end-labeled RNA is digested with nucleases that are structure and/or sequence specific. The digestion products are run on a gel along

with ladders and are then compared to the ladders in order to determine the position of each cut. The ladders are typically generated in two ways. The first is through alkaline hydrolysis which cleaves on the 3' side of a base and has the capability of producing a band corresponding to each nucleotide.[20] Often, a T1 ladder is also included. RNase T1 cleaves ssGpN residues, leaving a 3' phosphate.[21, 22] When incubated with T1 under denaturing conditions, every G residue in the RNA is available for cleavage. This ladder aids in the assignment of bands.[23]

Structure mapping can be completed with a number of nucleases. Two common RNases used for the procedure are T1 and V1. T1 is isolated from *Aspergillus orizae* and cleaves single-stranded guanine residues, leaving a 3' phosphate.[21, 22] The pattern of cleavage by this enzyme provides a general idea of which regions of the RNA are single stranded. It is important to consider the effect of modifications on the activity of this enzyme. Naturally modified m^1G and m^7G are not recognized by RNase T1.[21] The Pdases have a modified uracil, and it is possible that modified bases near single stranded G residues could interfere with enzyme activity.

RNase V1, obtained from cobra *Naja naja oxiana* venom, cleaves dsRNA.[21, 22] While V1 shows no base specificity, the enzyme requires a minimum of 4 to 6 nucleotides in helical conformation – 1 or 2 bases are needed on either side of the target site .[21, 22, 24] RNase V1 is also capable of cleaving single-stranded regions that are in a stacked conformation.[21, 24] The resulting fragments have a 3' hydroxyl.[22, 23] The difference between the 3' phosphate left by T1 and the 3' hydroxyl left by V1 results in V1 products with reduced mobility relative to T1 products.[23] While this complicates the assignment of bands in the samples treated with V1, the use of multiple ladders can help resolve this issue. RNase V1 is a useful enzyme for structure mapping because it is absolutely dependent upon magnesium for its function.[21, 22] Reactions with this enzyme can easily be terminated by the addition of EDTA, allowing for precise control in the experiment.

In each reaction for the structure mapping, it is important to optimize conditions so that the rate of cutting is low – ideally greater than 90% of the RNA remains intact.[22] This low level of cleavage reduces the probability that an RNA molecule will be cleaved more than once. This condition is important because after the first cleavage, the structure of the RNA may be altered. Any secondary cuts made will not necessarily provide an accurate picture of the true RNA structure.[21, 22] In order to optimize conditions, the RNA is incubated with a serial dilution of enzyme and the amount of enzyme that results in both a large amount of full length RNA and discernable and interpretable bands corresponding to the cleavage products is selected.

Results

Thermal Melting

Each sequence produced a characteristic melting curve and most had a well defined melting temperature. Point estimations for the melting temperature were determined by averaging the inflection points of cubic functions fit to melting experiments for each sequence. Experiments were repeated at least three times for each sequence. Though the melting temperatures reported were calculated using inflection points, calculations using midpoints resulted in similar values (results not reported). The melting curves are also analyzed for the percentage that the absorbance increases which is calculated by subtracting initial absorbance from the final absorbance then dividing by the initial absorbance. Each melting temperature and percent increase in absorbance is reported as a 90% confidence interval, calculated using t-scores. Unless otherwise noted, each melting experiment was performed in 50 mM phosphate buffer (pH 7) and the temperature ramp rate was 2°C/minute.

Pdase 17 (Family 1)

As seen in Figure 4, Pd 17 tends to steadily increase in absorbance as temperature rises. Though the absorbance seemed to be flattening somewhat near the lower temperatures, it is

practically very difficult to measure absorbance below 10°C because water condenses on the outside of the cuvette – this effect is seen in Figure 4 in the curve corresponding to temperature increase. The T_m for Pd 17 is less clearly defined than for other sequences due to the lack of sigmoidal shape. The melting temperature for modified Pd 17 is 55.99 ± 1.43 °C, and the percent increase in absorbance is 19.1 ± 6.9%.

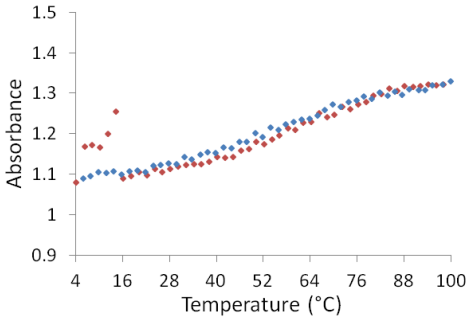

Figure 4. Characteristic Pd 17 melting curves. The red line corresponds to the curve produced when temperature is increased at a rate of 2°C/min and the blue curve was obtained while the temperature was decreasing at the same rate.

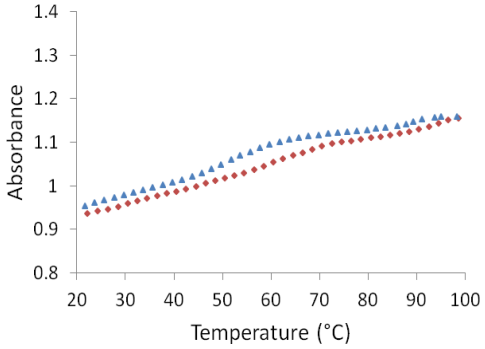

Figure 5. Characteristic unmodified Pd 17 melting curves. The red line corresponds to the curve produced when temperature is increasing the blue curve was obtained while the temperature is decreasing.

The melting curve produced by unmodified Pd 17 (Figure 5) has a slightly different shape than that of modified Pd 17. The curve has at least three transitions and shows a slight separation between the curve obtained over increasing temperature and the curve obtained during decreasing temperature. The T_m for unmodified Pd 17 is 56.21 ± 5.13°C, and the percent increase in absorbance is 25.4 ± 6.1%. The differences between the melting temperature and percent increases for modified and unmodified Pd 17 are not statistically significant.

Pdase 34 (Orphan)

The melting curve of Pd 34, shown in Figure 6, has a much different shape than that of Pd 17. The curve is a classic sigmoid with a separation between the curves corresponding to the ramp up and to the ramp down. The T_m for modified Pd 34 is 59.36 ± 0.24°C and the percent increase in absorbance is 43.7 ± 15.6%. The variation in the percent increase in absorbance correlates to the initial absorbance of the Pd 34 sample. A sample calculated to be 1.53 μM had the lowest percent increase in absorbance at 35.45%. A sample of 0.97 μM Pd 34 had a percent increase in absorbance of 44.6%, and the sample with the lowest concentration, 0.88 μM, had a percent increase in absorbance of 54%, which is the largest percent increase in absorbance.

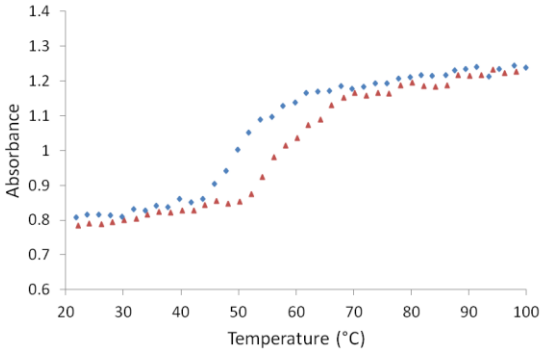

Figure 6. Characteristic modified Pd 34 melting curves. The red line corresponds to the curve produced when temperature is increased the blue curve was obtained while the temperature is decreasing.

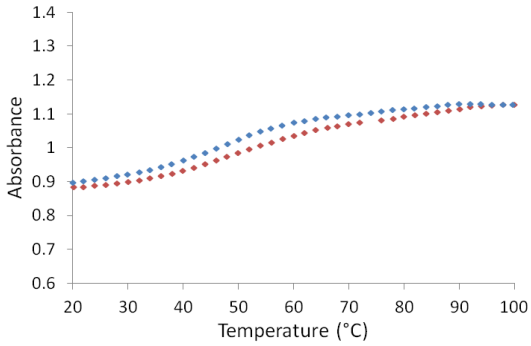

Figure 7. Characteristic unmodified Pd 34 melting curves. The red line corresponds to the curve produced when temperature is increased the blue curve was obtained while the temperature is decreasing.

Unmodified Pd 34 produced curves, shown in Figure 7, with a much lower change in absorbance. The average percent increase in absorbance was 27.0 ± 1.3%. Despite the large error for the percent increase for modified Pd 34, the difference between the modified and unmodified sequences is statistically significant at the level of α=0.02. Like the unmodified Pd 17 melting curve, unmodified Pd 34 showed at least three clear transitions with a slight separation between the ramp up and ramp down curves. The melting temperature for unmodified Pd 34 is

54.95 ± 3.00°C. The difference between the melting temperatures for modified and unmodified Pd 34 is statistically significant at the level of α=0.005

Pdase 20 (Family 3)

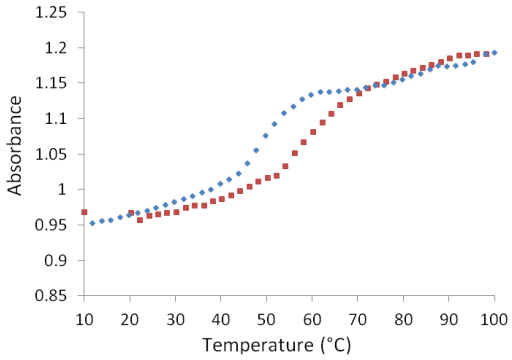

Figure 8. Characteristic modified Pd 20 melting curves. The red line corresponds to the curve produced when temperature is increased at a rate of 2°C/min the blue curve was obtained while the temperature is decreased at the same rate.

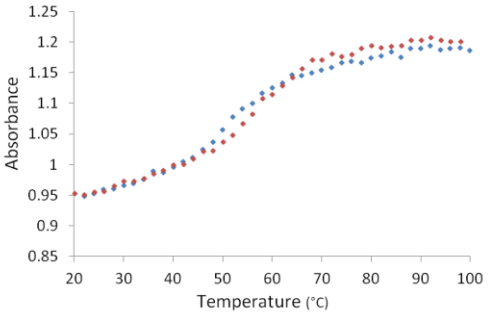

Figure 9. Characteristic modified Pd 20 melting curves. The red line corresponds to the curve produced when temperature is increased at a rate of 0.5°C/min the blue curve was obtained while the temperature is decreased at the same rate.

Like Pd 34, Pd 20 melting, shown in Figure 8, has a sigmoidal shape with a separation between the curves obtained during increasing temperature and those obtained during decreasing temperature. This separation does not exist when the RNA is melted at 0.5°C/minute, curves shown in Figure 9, rather than at 2°C/min. From the separation observed during melting of modified Pd 20, it is evident that the RNA folds more slowly than is allowed by the 2°C/min temperature change. The melting temperature for modified Pd 20 is 58.71 ± 1.09°C and the percent increase in absorbance is 29.3 ± 4.3%.

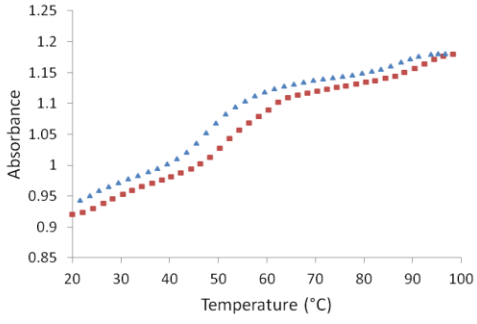

Figure 10. Characteristic unmodified Pd 20 melting curves. The red line corresponds to the curve produced when temperature is increased at a rate of 2°C/min the blue curve was obtained while the temperature is decreased at the same rate.

Figure 10 shows melting curves for unmodified Pd 20. While there is a slight separation in the curves, it is much less severe than the separation observed when modified Pd 20 is melted at a rate of 2°C/min. The overall

shape of the melting is also fairly different from that seen in modified Pd 20, with at least three clear transitions. This shape is very similar to the melting curves for unmodified Pd 34 and unmodified Pd 17.

Pdase 92 (Family 2)

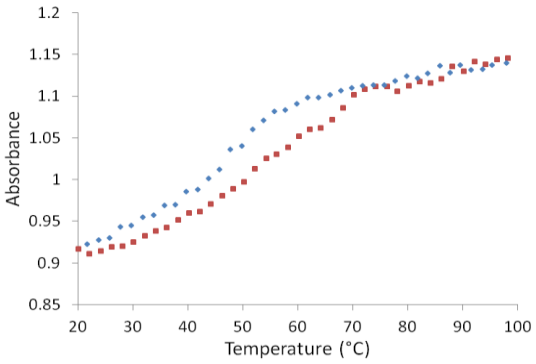

Figure 11. Characteristic modified Pd 92 melting curves. The red line corresponds to the curve produced when temperature is increased at a rate of 2°C/min the blue curve was obtained while the temperature is decreased at the same rate.

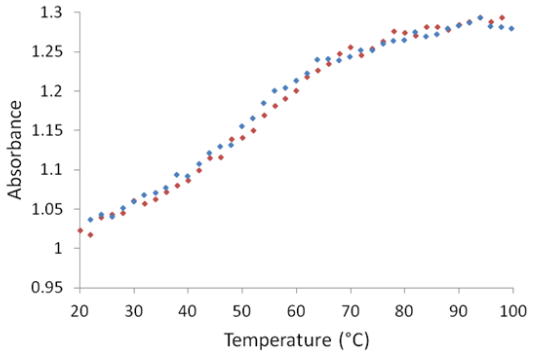

Figure 12. Characteristic modified Pd 92 melting curves. The red line corresponds to the curve produced when temperature is increased at a rate of 0.5°C/min the blue curve was obtained while the temperature is decreased at the same rate.

The melting curves for Pd 92, shown in Figure 11, also have a separation between the ramp up and ramp down curves; though, this separation is smaller than that for Pd 34 or Pd 20. While Pd 92 plateaus at both low and high temperatures, the curve is not as sigmoidal as Pd 20 or Pd 34. There are possibly multiple transitions in the melting curve for Pd 92. The T_m for modified Pd 92 is 54.98 ± 2.15°C and the percent increase in absorbance is 26.5 ± 4.0%. As with Pd 20, the separation between the curves was eliminated when Pd 92 was melted at a rate of 0.5°C/minute. These curves are shown in Figure 12.

Pdase 81 (Family 4)

Pd 81 melting, shown in Figure 13, is most similar to that of Pd 17. Melting for Pd 81 shows no clear transitions and does not plateau at low or high temperatures. The percent increase for Pd 81

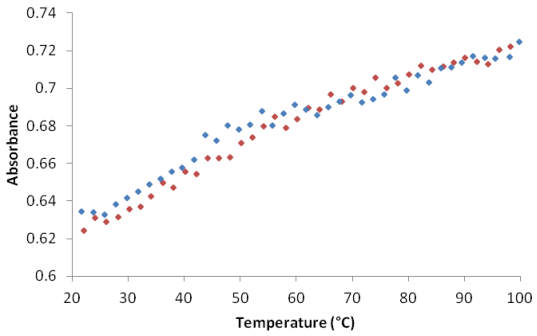

Figure 13. Characteristic modified Pd 81 melting curves. The red line corresponds to the curve produced when temperature is increasing the blue curve was obtained while the temperature is decreasing.

was calculated to be 15.9 ± 1.4%. Melting temperature was not calculated because Pd 81 has no clear transition. When cubic functions are fit to the data, no inflection point that is consistent with the midpoint can be calculated from the function. Because the melting curve shows no sign of plateauing at the low or high temperature range, it is possible that the percent increase in absorbance is actually higher than 16%. Because of this uncertainty, melting temperature could not be reliably calculated based on the midpoint technique.

Salt Effects

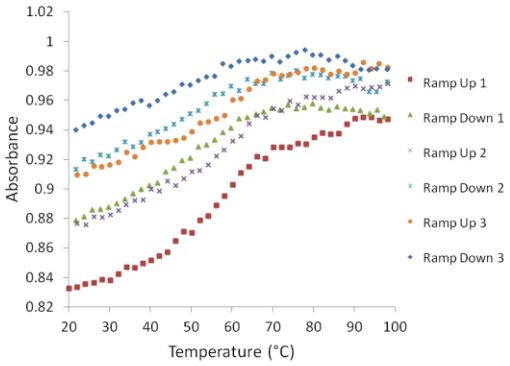

Figure 14. Melting curves for Pd 17 obtained in 1mM Phosphate Buffer. The red curve was obtained during the first temperature increase.

When Pd 17 was melted in 1mM Sodium Phosphate Buffer, shown in Figure 14, the melting curve during the first temperature increase was similar to the curves observed for Pd 17 in 50mM Sodium Phosphate Buffer. However, the melting curve for the first temperature decrease failed to return to the starting absorbance. The melting curves after this showed the same trend. The percent increase in absorbance for the first melting curve was about 14.3%, which is within error for the average percent increase in absorbance for modified Pd17. However, the percent change in absorbance on the melting curve collected during the final temperature decrease was only 4.2%. Similar results were obtained in a repeat of this experiment, with the increase in absorbance on the first melting curve at about 16.0% and the percent change in absorbance on the final curve at only 6.4%. Likely, the RNA was able to fold correctly in 1mM phosphate buffer, as indicated by the first ramp up, but was unable to refold properly after melting.

Summary

Overall, the modified Pdases each showed characteristic melting curves that were sequence dependent. The unmodified melting curves were different from the curves for their modified

counterparts. However, the unmodified melting curves were similar to each other, each showing at least three transitions. The melting temperatures and percent increase in absorbance for selected sequences are summarized in Table 1.

Sequence	T_m (°C)	Percent Increase in absorbance
Pd 17	55.99 ± 1.43	19.1 ± 6.9
Pd 17 unmodified	56.21 ± 5.13	25.4 ± 6.1
Pd 20	58.71 ± 1.09	29.3 ± 4.3
Pd 92	54.98 ± 2.15	26.5 ± 4.0
Pd 34	59.36 ± 0.24	43.7 ± 15.6
Pd 34 unmodified	54.95 ± 3.00	27.0 ± 1.3
Pd 81	inconclusive	15.9 ± 1.4

Table 1. Melting temperature and percent increase in absorbance for each sequence averaged for at least 3 samples with error calculated at 90% confidence. Unless otherwise noted, the data is from sequences with modified uracil bases.

If the Pdases formed bimolecular or multimolecular interactions, the T_m should increase as concentration increases. This trend was not observed – melting temperature appears to be concentration independent. Therefore, the Pdases likely fold via intramolecular interactions.[14] This indicates that the inflection point method for determining melting temperature is a valid method to analyze the Pdase melting curves.

Circular Dichroism

The circular dichroism spectrum for each RNA studied was highly reproducible. Both the amplitude and position of major peaks remained nearly constant across each trial, with the spectrums overlapping almost perfectly. By comparing these spectra to each other and to spectra of nucleic acids with known structures, it is possible to gain insight into the structure of the Pdases and how they compare to each other. All data is reported with a 90% confidence interval, calculated using t-scores. Unless otherwise noted, each experiment was performed in 50 mM phosphate buffer and the temperature was held at room temperature (about 21°C).

Modified Pdases

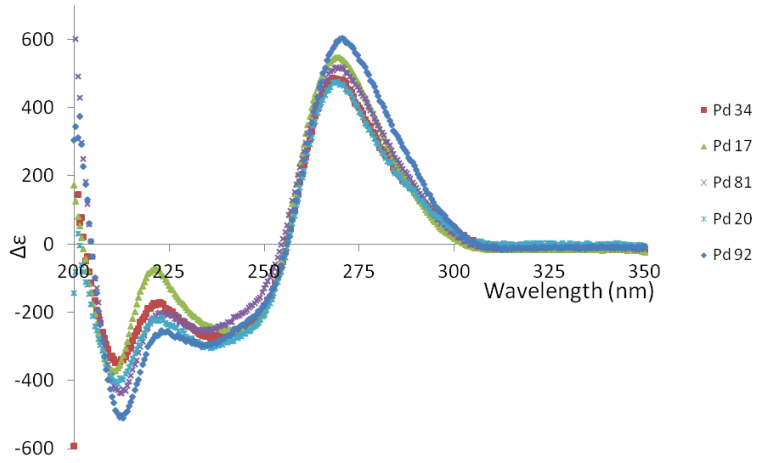

Figure 15. Characteristic circular dichroism spectrum for each modified Pdase normalized for concentration and pathlength

As seen in Figure 15, the circular dichroism spectra for each of the five sequences selected have a similar shape. The locations of the maximum and minimum peaks are summarized in Table 2. The location of the positive peaks ranges from 268.25 nm to 270.6 nm and the sequences each have a well-defined minimum peak near 210nm.

Sequence	Maximum (wavelength - nm)	Minimum (wavelength - nm)
Pd 17	269.7 ± 0.5	210.8 ± 1.0
Pd 17 unmodified	267.8 ± 0.5	208.8 ± 1.3
Pd 20	270.0 ± 0.8	212.3 ± 1.3
Pd 92	270.5 ± 0.0	212.5 ± 3.2
Pd 34	268.25 ± 1.6	211.3 ± 1.6
Pd 34 unmodified	266.5 ± 0.0	208.8 ± 1.3
Pd 81	270.6 ± 0.7	212.0 ± 0.4

Table 2: Positions of the maximum and minimum peaks for the circular dichroism spectra of each Pdase averaged for at least 2 trials with error calculated at 90% confidence using t-scores.

The shapes of the Pdase spectra are similar to that of A-form RNA which has a maximum near 260 nm and a minimum near 210 nm.[13, 17] The maximum peak is slightly shifted from the typical A-form RNA spectrum to a maximum closer to that seen in A-form DNA. While the general peak positions and shapes of the spectra are similar to that of A-form RNA, the differences suggest that the RNA is not simply a pure A-form helix.

Unmodified Pdases

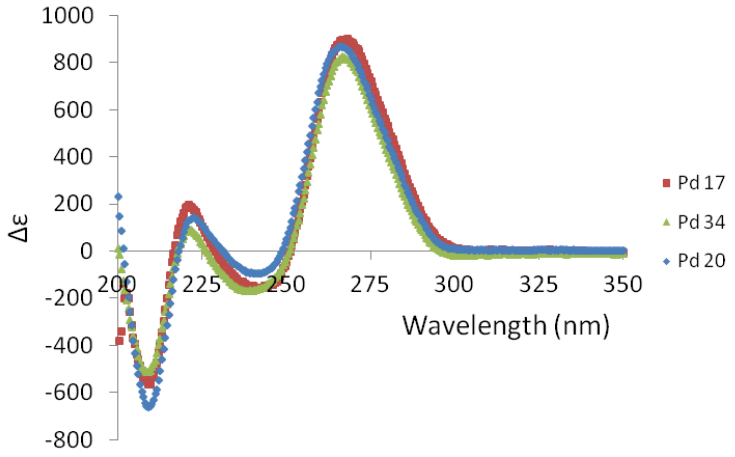

Figure 16. Characteristic circular dichroism spectrum for selected unmodified Pdase normalized for concentration and pathlength

Figure 16 shows the characteristic circular dichroism spectra for selected unmodified Pdases. Like the modified Pdases, the shapes of the spectra are similar to those of A-form nucleic acids, with maxima between 266 nm and 268 nm and minima near 210nm. The maximum and minimum peak positions are listed in Table 2.

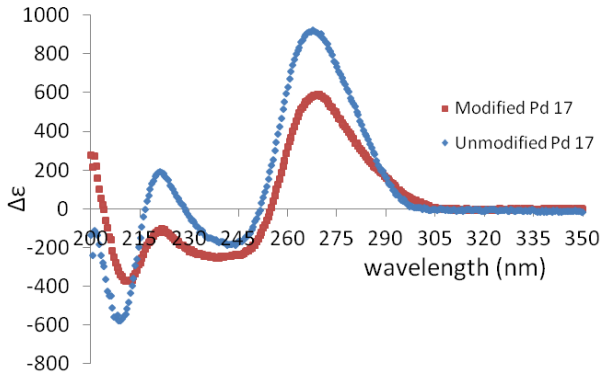

Figure 17. Overlay of the circular dichroism spectra for modified and unmodified Pdase 17.

Though the general shapes of the modified and unmodified Pdase spectra are similar, the amplitudes of their peaks are very different. It is evident from the overlay of the spectra, shown in Figure 17, that the incorporation of modified uracil residues significantly changes the circular dichroism spectrum of the RNA. The unmodified Pdase spectra are much more similar to each other than they are to their modified Pdase counterparts. This change in circular dichroism spectrum likely corresponds to changes in the structure of the RNA.

Circular Dichroism and Melting

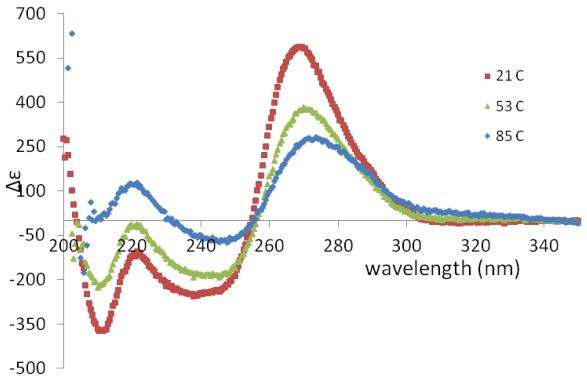

Figure 18. Circular dichroism spectra for Pd 17 at 21 °C, 53°C, and 85°C

Circular dichroism spectra for Pd 17 were collected at 21°C, 53°C and 85°C; these spectra are shown in Figure 18. 53°C was chosen because it is near the melting temperature for Pd 17 and at 85°C, it is believed that the RNA exists mostly in its unfolded state. Compared to 21°C, at 85°C the circular dichroism spectrum for Pd 17 is more similar to that of single-stranded, unstructured RNA.[15] This trend is to be expected and indicates that the spectrum observed at room temperature corresponds to a folded RNA structure that is disrupted upon melting.

Structure Mapping

In order to gain more insights to the structure of the Pdases, structure mapping, using RNase V1 and T1, can be performed on a selection of Pdases. In preparation for structure mapping, RNA was 5' end-labeled using T4 polynucleotide kinase and γ^{32}P-ATP.

Control Hairpin

Prior to work with Pd 17, a control hairpin was designed to test the function of the enzymes, especially with regard to the modified bases, and to determine conditions for the experiments. The control hairpin contained only three uracil residues in order to increase the

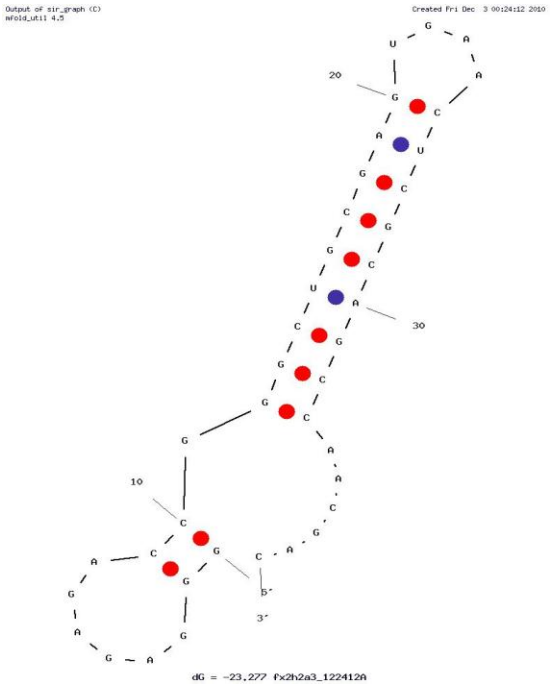

Figure 19. Structure of the control hairpin predicted using IDT OligoAnalyzer.

likelihood that the RNA folded into the expected hairpin structure. The hairpin sequence is 5'-GGGAGAGACCGGGCUGCGAGUGAACUCGCAGCCAACGAC-3'. Primers were designed for maximum binding to the DNA template while minimizing primer-dimers and off target binding. This analysis was completed using the IDT OligoAnalyzer tool. The predicted structure of the hairpin from the IDT OligoAnalyzer is shown in Figure 19. The loop has one guanine residue which should be susceptible to cleavage by T1, and the stem region should be susceptible to cleavage by V1. Both modified and unmodified versions of the hairpin were used for structure mapping.

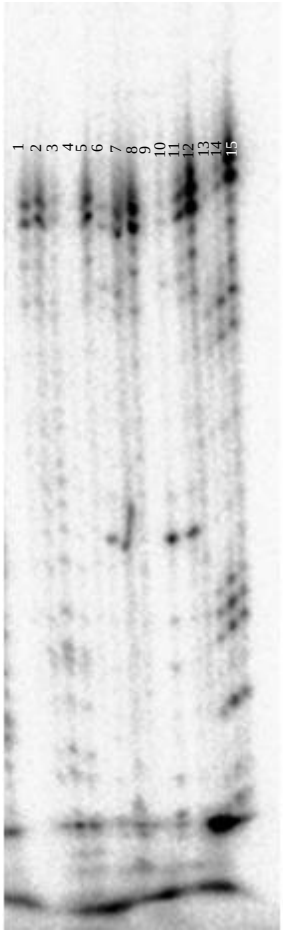

Figure 20. Structure map of the modified hairpin. Lane 1: labeled hairpin RNA; Lane 2: Alkaline hydrolysis, 2 min incubation; Lane 3: Alkaline hydrolysis, 5 min incubation; Lane 4: Alkaline hydrolysis, 15 min incubation; Lane 5: T1 ladder, 0U; Lane 6: T1 ladder, 1.0U; Lane 7: T1 ladder, 0.1U; Lane 8: T1, 0U; Lane 9: T1, 1.0U; Lane 10: T1, 0.1U; Lane 11: T1, 0.01U; Lane 12: V1, 0U; Lane 13: V1, 0.1U; Lane 14: V1, 0.01U; Lane 15: V1, 0.001U

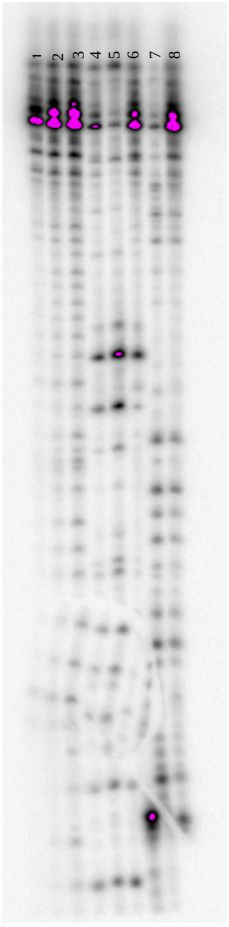

Figure 21. Structure map of the unmodified hairpin. Lane 1: labeled hairpin RNA; Lane 2: Alkaline Hydrolysis, 2 min incubation; Lane 3: Alkaline hydrolysis, 3 min incubation; Lane 4: T1 Ladder, 0.1U; Lane 5: T1, 0.1U; Lane 6: T1, 0.01U; Lane 7: V1, 0.01U; Lane 8: V1, 0.001U

Structure mapping on the modified hairpin, shown in Figure 20, resulted in one strong T1 cleavage site (lanes 10 and 11), assumed to correspond to the guanine residue in the hairpin's loop. There were also strong V1 cleavage sites (lanes 13-15) on either side of the T1 site, likely created by RNase cuts in the stem region of hairpin. Unfortunately, the alkaline hydrolysis ladder was not complete enough to use for true band assignment. The gel resolution could also be much improved. The samples appear as dots rather than bands and there is some graininess in the gel. The results, however, were enough to determine that both RNase T1 and V1 were functioning as expected.

Structure mapping of the unmodified version of the hairpin was completed using slightly different conditions. The 36 well comb used in the modified hairpin experiments was replaced with a 20 well comb which creates wider wells. The unmodified hairpin experiments were also performed with new pipette tips that have a flat end 0.17mm in thickness. This allowed samples to be placed directly on the gel rather than dropped into the well. Fresh gel stock was used to ensure good gel resolution. Finally, the stop conditions for the reactions were modified. The reactions were stopped by the addition of unlabled yeast RNA (4 μg) and EDTA (1mM) followed by heating the sample at 95°C for 2 minutes, rather than stopped just with heat and EDTA.

The structure mapping of the unmodified hairpin, shown in Figure 21, confirmed the results obtained from the modified hairpin. Digestion with T1 (lanes 4-6) resulted in 2 clear bands and V1 digestion (lanes 7 and 8) resulted in cuts in regions not susceptible to T1. Only one T1 band was expected, but the extra band could be a result of the digestion of non-full-length RNA or digestion of partially unfolded RNA. The alkaline hydrolysis ladder for the unmodified hairpin was much more complete than that in the modified experiment and the gel had much better resolution with RNA appearing as clear bands. The RNA, however, was not completely pure which complicates analysis of the gel. Additionally, the gel ripped in the lower portion, again complicating analysis. Overall, from both hairpin experiments, it is appears that the RNases are functioning as expected and the gel images provide enough resolution to interpret the digestion result, though resolution could be improved further by increasing the percentage of bis-acrylamide in the gel. Structure mapping on Pdases has been complicated due to degradation of the RNA samples, but moving forward, structure mapping has the capability of providing great structural insight into the RNAs.

Discussion

Thermal Melting

From the melting data, it is evident that each of the Pdases folds into a structure that minimizes the overall dipole of the molecule. The increase in absorbance on each of the melting curves is larger than what may be accounted for by normal drift in absorbance as temperature rises, especially in light of the fact that the absorbance of the phosphate buffer is subtracted from the absorbance of the nucleic acid at each temperature point. It is therefore clear that each of the Pdases studied folds into an ordered structure. Because the T_m does not appear to be concentration dependent, the Pdases fold via intramolecular interactions.[14] Furthermore, due to differences in the melting curves, it is likely that the Pdases do not have identical structures.

Pd 34, Pd 20, and Pd 92 each showed a separation between the melting curves produced during periods of increasing temperature and those produced during decreasing temperature. When the rate of temperature change was reduced from 2°C/min to 0.5°C/min, this separation was eliminated for both Pd 20 and Pd 92 (experiments at the lower temperature ramp rate were not performed on Pd 34). While 2°C/min did not provide enough time for the RNA to fold, the slower rate allowed the Pdases to properly fold at each temperature point.

Though Pd 17 and Pd 81 were able to fold on the time scale of 2°C/min, that is, the melting curves did not contain an apparent separation, the melting curves produced by these Pdases were not sigmoidal in shape. Instead, both melting profiles show a steady increase in absorbance with a very slight leveling off for Pd 17 but not for Pd 81. The sigmoidal shape in melting curves arises due to cooperative melting – as a duplex begins to come apart, the whole structure is destabilized and the remaining base pairing interactions dissociate rapidly. Multiple transitions in a melting curve typically correspond to the unfolding of tertiary structures.[14, 15] The lack of a clear sigmoidal curve for Pd 17 and Pd 81 melting may be due to multiple structural motifs contributing to RNA folding rather than one duplex interaction. The more linear nature of the melting profiles would, in this case,

be the result of many transitions in the melting profile caused by unfolding of these structural motifs.

While the melting curves corresponding to the modified Pdases were all different from each other, the melting curves produced by the unmodified Pdases were all very similar. They each contained three obvious transitions with a very slight separation between the ramp up and ramp down melting curves. Even without the modified uracil residues, the Pdases produce melting curves different from the classic sigmoidal curve which is observed during the melting of a double stranded helix. It is evident that the unmodified Pdases fold into different structures than their modified counterparts and that they may not fold only into simple helical structures.

Accounting for Error in Pd 34 Data

The percent increase in absorbance for Pd 34 was much higher in error (15.6%) than any of the other measurements. In the three repetitions of Pd 34 melting, the RNA sample with the lowest RNA concentration resulted in the highest percent increase in absorbance while the sample with the highest RNA concentration resulted in the lowest percent increase in absorbance. One explanation for this trend may be that in the samples with the lowest calculated concentration, more of the RNA was properly folded. With more RNA in the properly folded state, the initial absorbance measurement would be lower than if the sample contained misfolded or unfolded RNA. Also, with more properly folded RNA molecules unfolding, the total increase in absorbance for the sample would be higher; if RNA is misfolded or partially unfolded, its overall dipole does not increase as much upon unfolding, resulting in a lower percent increase in absorbance for the sample. If this is the reason behind the trend observed for percent increase in Pd 34 melting, the higher percent increases represent a more accurate estimation of the true change in absorbance.

Salt and Folding

When Pd 17 was melted in 1mM phosphate buffer rather than 50mM phosphate buffer, the melting curve produced during the first period of increasing temperature was standard in shape and percent change in absorbance. However, each melting curve after the first showed a progressively higher absorbance at room temperature and a progressively lower percent change in absorbance, with the final melting curve only showing a 4.2% increase in absorbance.

This data suggests that in 1mM phosphate buffer, the RNA is able to adopt a properly folded confirmation, but after being subjected to melting, the RNA is unable to refold properly. While the salt concentrations used in the preparation of the Pdases is sufficient for folding under normal conditions, the RNA requires more salt to refold after being treated with harsh melting experiments.

Circular Dichroism

The circular dichroism spectrum for each sequence studied was highly reproducible. This is reflected in the low error for each of the maximum and minimum peaks in the spectra. The spectra for the modified Pdases were all similar to that of A-form nucleic acid. The spectra did not, though, fit perfectly to the standard A-form RNA spectrum. The maximum peak for each spectrum was red shifted toward the wavelengths typically seen for A-form DNA (270nm).[13] It is therefore likely that the Pdases contain some helical structure, but are not purely A-form RNA. The slight variations between the spectra suggest that the structures of the Pdases are not identical.

The spectra for the unmodified Pdases showed similar peak positions to their modified counterparts. The amplitudes of the peaks were, however, much greater for the unmodified Pdases. The positive peak around 270nm is sensitive to winding angle. One study found an average decrease in CD of 3.2 ± 0.1 M^{-1} cm^{-1} per 1° increase in winding angle.[12] The large amplitude difference at this peak suggests that modified Pdases have a larger winding angle, i.e. fewer bases per turn, than their unmodified counterparts. Additionally, the spectra for the unmodified Pdases contain a second

positive peak while that same minor peak remains below the axis in the modified spectra. These large differences between the spectra for modified and unmodified Pdases indicate that the modified uracil residues change the structure of the RNA.

Structure Mapping

Structure mapping completed on a hairpin designed to contain only three uracil residues confirmed the specificity of RNase T1 for single stranded guanine residues and the specificity of RNase V1 for double stranded regions of RNA. RNase T1 cannot cleave certain naturally modified G residues in tRNA, so it was important to test the ability of the enzymes to cleave at or near modified uracil bases.[21] The hairpin controls demonstrated the ability of both enzymes to cleave near the modified uracil residues. Though the controls with the modified RNA were successful, it was more difficult to generate a complete alkaline hydrolysis ladder, even with higher incubation times. To remedy this issue, an alkaline hydrolysis ladder generated from the unmodified RNA can be run on the same gel as the modified structure mapping reactions in order to aid with band assignment. The hairpin controls were important for both testing the abilities of the enzyme and for optimizing reaction and gel conditions and gel loading techniques.

Unfortunately, structure mapping on modified Pd 17 was not completed due to issues with degradation of the RNA. The creation of new beads for transcription and the use of new alkaline phosphatase (to reduce the likelihood of RNases present in the enzyme solution) did not resolve the issues. Rather than attempting phosphatase reactions followed by end-labeling, future experiments may employ a kinase-exchange reaction, which eliminates the alkaline phosphatase step, to reduce the likelihood of RNA degradation.

Conclusions

Overall, analysis of the five Pdase isolates in their modified and unmodified forms by thermal melting, circular dichroism, and structure mapping provided many insights into the

structures of the RNAs. The thermal melting curves, due to a relatively slow rate of folding and the presence of multiple transitions in some of the melting curves, indicate that the Pdases each contain structures that likely involve non-Watson Crick interactions. The thermal melting data also indicates that the Pdases are not identically structured and that the modified versions of the RNA fold into different structures than the unmodified versions of the RNA.

Circular dichroism data confirmed some of these conclusions and also provided new insights. From the differences in the circular dichroism spectra, it is evident that the Pdases are not identically structured nor do the RNAs have the same structures if unmodified uracil is used in place of 5-(4-pyridylmethyl)-uracil. Furthermore, the spectra of the Pdases are very similar to the spectrum of A-form RNA, though there are slight differences in the position of the positive peak. This similarity indicates that the RNAs contain A-form structures, but the differences suggest that that the RNA is not simply a pure A-form helix.

Finally, structure mapping is able to provide more detailed information about the structured regions of the RNA. A control hairpin containing only three uracil residues was used to test the ability of the enzymes to cleave at or near the modified uracil bases and to determine proper experiment conditions. Structure mapping on modified Pdases has been unsuccessful due to degradation of the RNA, but new techniques may be used to alleviate this issue including a kinase exchange reaction to replace the phosphatase and end-labeling sequence of reactions.

From these studies, it is evident that the Pdases fold into highly ordered structures dictated by their primary sequences and that these structures involve non-Watson Crick interactions. Further studies with NMR or X-ray crystallography would provide even more detail about the precise structures of the RNAs and how they compare to one another. Furthermore, studies on RNA bound to palladium particles have the potential to provide much more information about the functionality of the RNAs. RNase footprinting on RNA bound to particles would identify the

portion of the RNA that interacts with the palladium nanoparticle. By determining these sites, it may be possible to design RNA molecules that are better at mediating particle growth. If Pd 34, which mediates cubic particles, were analyzed and compared to Pdases that mediate hexagonal particle growth, it might even be possible to determine the mechanism for control of particle shape. One can imagine that it might be possible to design Pdases that mediate nanoparticle growth with a desired shape specificity and high efficiency. Understanding how structure contributes to function of the Pdases can lead to much deeper understanding of how they mediate their chemistries, to the development of better RNA catalysts, and to new materials applications.

Experimental Section

Sample Preparation

RNA was transcribed from biotinylated dsDNA immobilized on streptavidin coated beads using T7 RNA Polymerase (450 Units), ATP, CTP, GTP, and 5-(4-pyridylmethyl)-UTP (0.9 μM each). DNA templates and primers were synthesized on an oligosynthesizer using standard methods. The RNA transcription products were purified on an 8% denaturing polyacrylamide gel (19:1 acrylamide:bis-acrylamide) followed by passive elution in EDTA (2mM, pH 7). EDTA was removed from the solution by washing on 30,000 MWCO Millipore AmiconUltra cellulose spin columns. The RNA was then washed twice with 300 μL NaCl, KCl, $MgCl_2$, $CaCl_2$, and Na_2HPO4 (1mM each, pH 7). Five 300 μL water washes followed to remove excess salt. Unmodified RNA samples were prepared using the same method, but unmodified UTP replaced 5-(4-pyridylmethyl)-UTP in the procedure.

The purity of RNA samples was assessed using 8% polyacrylamide gels with a 10bp DNA ladder in one lane, unpurified transcription product of the sequence in another, and the purified RNA sample in a third lane. Gels were stained with SyberGold and imaged with a 473nm laser.

RNA was considered pure if there were no observable bands other than the band corresponding to full length RNA.

Final samples for thermal melting experiments were prepared with RNA (about 1 μM) in phosphate buffer (50mM). Samples for circular dichroism were also in phosphate buffer (50mM), and were between 0.2 and 0.5μM in RNA concentration.

Thermal Melting

RNA samples were placed in a 10mm pathlength quartz cuvette. Absorbance of 260 nm light by the RNA samples was collected from 20 to 100°C at a rate of 2°C/min, with the exception of the Pd 20 and Pd 92 melting curves that were collected at 0.5°C/min. Spectra for each Pdase were collected at least 3 times and each experiment consisted of three ramp up and three ramp down repeats. Melting curves were normalized by subtracting the absorbance of 50mM phosphate buffer from the sample's absorbance. The melting data was collected on a Cary 100 spectrophotometer.

Melting temperatures were determined by fitting a cubic function to the melting data and determining the inflection point. The melting temperatures for each sequence were averaged across the multiple trials. 90% confidence intervals were calculated using a t-distribution due to the relatively small number of data points for the melting temperature. Outliers were removed before calculations were performed.

Circular Dichroism

Circular dichroism spectra were obtained from 200-350nm at 0.5 nm per step and 10 seconds per step. Samples were held at room temperature (about 21°C) for the experiments except for the CD experiments completed on melted Pd 17 which were performed at 53°C and at 85°C. Spectra were normalized by subtracting background absorbance from the sample absorbance. Spectra were collected on an Applied Photophysics ChirascanPlus Circular Dichroism and Fluorescence Spectrometer. 90% confidence intervals for the position of the maximum peak and

minimum peak were calculated for each sequence using a t-distribution. Outliers were removed before any calculations were performed.

Structure Mapping

RNA (20 pmol) that had been gel purified and washed with salt on 30K molecular weight cutoff microcons was mixed with 10x dephosphorylation buffer (50mM Tris-HCl (pH 9.3 at 25°C), 1mM MgCl2, 0.1mM ZnCl2 and 1mM spermidine), and calf intestine alkaline phosphatase (1U) in order to remove the 5' phosphate. The mixture was incubated at 37°C for 1 hour and stopped with EDTA (1mM) and heating at 65°C for 5 minutes. The reaction was washed on GE Healthcare G-50 microcolumns to remove the EDTA and excess salts. The CIAP reaction was then mixed with γ^{32}P ATP (25pmol) (6000 Ci/mmol), buffer (50 mMTris (pH 8.5), 10mM $MgCl_2$, 5mM DTT), and T4 Polynucleotide Kinase (0.1U). The reaction was incubated for 1 hour at 37°C, stopped with ETDA (1 mM) and 95°C heat, then washed on microcolumns. Purity of the end-labeled RNA was assessed using 12% denaturing polyacrylamide gel electrophoresis. The RNA was treated with gel purification and passive elution if not pure. If pure, the RNA was washed and treated with salt on 30k molecular weight cutoff microcons prior to structure mapping experiments.

The 5' end labeled RNA was digested in 4 different ways. In the first condition, RNA (3pmol) was incubated Alkaline Hydrolysis Buffer (50mM $NaHCO_3/NaCO_3$ pH 9.2, 1 mM EDTA) and yeast RNA (1 μg). The reaction was incubated at 95°C to a time that resulted in about one cleavage per 10 RNA molecules. In the second condition, RNA (4 pmol) and yeast RNA (1 μg) in denaturing buffer (20mM sodium citrate (pH 5), 1mM EDTA, 7M Urea) was heated at 65° for 5 minutes then incubated with T1 RNase (units are indicated in the results for each experiment) at room temperature, in order to generate a ladder with a band at every G residue in the RNA sequence. The third and fourth conditions were incubation at room temperature with T1 or V1 under non-denaturing conditions. RNA (4 pmol), yeast RNA (1 μg), and 10x RNA structure buffer

(100 mM Tris, pH 7, 1 M KCl, 100 mM $MgCl_2$) were incubated with T1 or V1 (units indicated for each experiment in the results section) at room temperature for 15 minutes. All T1 and V1 reactions were stopped by the addition 1mM EDTA and 4 μg yeast RNA and heated to 95°C. Each sample was mixed with 6μl gel loading buffer (15% formamide, 18mM EDTA, 0.025% SDS, xylene cylanol, bromophenol blue).

The samples were run on a 50 cm sequencing gel for 2.5 hours at 50 watts to achieve 1 base resolution. The gel was imaged in a Fuji-film IP cassette and the cassette was imaged using a 635nm laser.

Citations

1. Cech, T. (2002). Ribozymes, the first 20 years. *Biochemical Society Transactions, 30* (6), 1162 – 1166.

2. Doudna, J., and Cech, T. (2002). The chemical repertoire of natural ribozymes. *Nature, 418*, 222 – 228.

3. Wu, Q., Huang, L., and Zhang, Y. (2009). The structure and function of catalytic RNAs. *Sci China C Life Sci, 52* (3), 232-244.

4. Talini, G., Gallori, E., and Maurel, M. (2009). Natural and unnatural ribozymes: Back to the primordial RNA. *Research in Microbiology, 160*, 457-465.

5. Tarasow, T., Tarasow, S., and Eaton, B. (1997). RNA-catalysed carbon-carbon bond formation. *Nature, 389*, 54 – 57.

6. Tarasow, T., and Eaton, B. (1998). Dressed for Success: Realizing the Catalytic Potential of RNA. *Biopolymers, 48*, 29-37.

7. Zimmermann, B., Bilusic, I., Lorenz, C., and Schroeder, R. (2010). Genomic SELEX: A discovery tool for genomic aptamers. *Methods*, *52*, 125-132.

8. Taouji, S., et al. (2011). Advances in binder identification and characterization: the case of oligonucleotide aptamers. *New Biotechonology*, *0*(0), 1-5.

9. Vaught, J., Dewey, T., and Eaton, B. (2004). T7 RNA Polymerase Transcription with 5-position Modified UTP Derivatives. *J. AM. CHEM. SOC., 126*, 11231-11237.

10. Gugliotti, L., Feldheim, D., and Eaton, B. (2004). RNA-Mediated Metal-Metal Bond Formation in the Synthesis of Hexagonal Palladium Nanoparticles. *Science, 304*, 850 – 852.

11. Gugliotti, L., Feldheim, D., and Eaton, B. (2005). RNA-Mediated Control of Metal Nanoparticle Shape. *J. AM. CHEM. SOC., 127*(50), 17815 – 17818.

12. Guo, P. (2010). The Emerging Field of RNA Nanotechnology. *Nat Nanotechnol., 5*(12), 833-842.

13. Bloomfield, V. A., Crothers, D. M., & Tinoco, I. (2000). *Nucleic acids: structures, properties, and functions*. Sausalito: University Science Books.

14. Mergny, J., and Lacroix, L. (2003). Analysis of Thermal Melting Curves. *Oligonucleotides, 13,* 515-537.

15. Shi, P., Brinton, M., Veal, J., Zhong, Y., and Wilson, W. (1996). Evidence for the Existence of a Pseduoknot Structure at the 3' Terminus of the Flavivirus Genomic RNA. *Biochemistry, 35*, 4222-4230.

16. Sprecher, C., Baase, W., and Johnson, W. (1979). Conformation and Circular Dichroism of DNA. *Biopolymers, 18*, 1009-1019.

17. Kypr, J., Kejnovská, I., Renčiuk, D., and Vorlíčková, M. (2009). Circular dicroism and conformational polymorphism of DNA. *Nucleic Acids Resarch, 37*(6), 1713 – 1725.

18. Kypr, J., and Vorlíčková, M. (2002). Circular Dichroism Spectroscopy Reveals Invariant Conformation of Guanine Runs in DNA. *Biopolymers (Biospectroscopy), 67*, 275 – 277.

19. Miller, and Miller. (2004). *John E. Freunds's Mathematical Statistics with Applications*. Upper Saddle River: Pearson Prentice Hall.

20. Wurst, R., Vournakis, J, and Maxam, A. (1978). Structure Mapping of 5'-^{32}P-Labeled RNA with S1 Nuclease. *Biochemistry, 17*(21), 4493 – 4499.

21. Ehresmann, C., *et al.* (1987). Probing the structure of RNAs in solution. *Nucleic Acids Research, 15* (22), 9109 – 9128.

22. Clarke, P. (2010). RNA Footprinting and Modification Interference Analysis. *Methods in Molecular Biology, 118*, 73 – 91.

23. Brown, T., and Bevilacqua, P. (2005). Method for assigning double-stranded RNA structures. *BioTechniques, 38* (3), 368 – 372.

24. Harrison, G., and Lever, A., (1992). The human immunodeficiency virus type 1 packaging signal and major splice donor region have a conserved stable secondary structure. *Journal of Virology, 66* (7), 4144 – 4153.

25. Azimi, H. (2009). An exploration of the structure of Pdase 17 & Pdase 24 by thermal melting & circular dichroism: thesis for departmental honors in chemistry & biochemistry.

26. Banerjee, I. A., Yu, L., and Matsui, H. (2003). CU nanocrystal growth on peptide nanotubes by biomineralization: Size control of Cu nanocyrstals by tuning peptide conformation. *PNAS, 100*(25), 14678-14682.

27. El-Sayed, M. (2001). Some inetersting properties of metals confined in time and nanometer space of different shapes. *Acc. Chem. Res., 34* (4), 257-264.

28. Krishna, H., and Caruthers, M. (2011). Solid-Phase Synthesis, Thermal Denaturation Studies, Nuclease Resistance, and Cellular Uptake of (Oligodeoxyribonuleoside)methylborane Phosphine-DNA Chimeras. *J. Am. Chem. Soc., 133*(25), 9844-9854.